COMP9517 Computer Vision Project Report

Jatin Gupta
School of Computer Science and
Engineering,
University of New South Wales
Sydney, Australia
z5240221@student.unsw.edu.au

Karan Inder Singh
School of Computer Science and
Engineering,
University of New South Wales
Sydney, Australia
z5232648@student.unsw.edu.au

Marhadiasha Kusumawardhana
School of Computer Science and
Engineering,
University of New South Wales
Sydney, Australia
z5226934@student.unsw.edu.au

Shubhankar Mathur
School of Computer Science and
Engineering,
University of New South Wales
Sydney, Australia
z5225093@student.unsw.edu.au

Yash Tamakuwala
School of Computer Science and
Engineering,
University of New South Wales
Sydney, Australia
z5248584@student.unsw.edu.au

I. INTRODUCTION

Cells are the fundamental building blocks of life. Their movement, growth, duplication, and division are essential to the growth and maintenance of a living organism. Observation of their behaviour is important to understand the machinery of a living organism and also to understand how a disease starts and progresses. This observation includes counting their number and tracking their movement using a large number of time-lapse microscopy images. Manually doing this observation is labour-intensive and time-consuming. Hence, computer vision methods are very useful for this task [1].

Automated cell tracking has its own set of challenges. Different types of images require different image acquisition techniques. Cell properties such as – size, shape, motion and overlap make the task complex. Density of population and uneven image illumination only make it more challenging. Modelling techniques such as Kalman or particle filter have been known to be invalid as cell motion is random and can't be predicted.

In this project, we aim to use computer vision techniques to track cell movement and division on three image sequences captured using time-lapse microscopy. We are given 4 image sequences in each of Phase Contrast (PhC), Differential Interference Contrast (DIC) and Fluorescence (Fluo) microscopy imaging techniques. The intensity distribution largely differentiates the three of them. This in turn will determine the different preprocessing methods required to ease segmentation in each of them.

In this project, we have three tasks to accomplish. The first task is to segment individual cells and track their movement over time. The second task is to detect any mitosis events that happen at each frame. Lastly, the third task is to show four metrics for a selected cell at any frame.

For the first task, a sequence of microscopy images is read by the application and cells are detected. The detection should be visualized by a bounding box around each of the detected cell. The application should also track the trajectory of the movement of the cells. Lastly, the application should be able to display the real-time count of detected cells.

In the second task, the process of cell division called mitosis should be detected by the application and visualized by a differently coloured bounding box. Post-mitosis, the cells must be considered new cells. The application should also display the real-time count of cells that are undergoing mitosis in each frame.

For the third task, the user should be able to click on any of the cells to display information about the cell. This information includes the speed of the cell which is essentially the Euclidean distance between the coordinates of the cell's bounding box's centre in the current frame and the previous frame. Total distance, net distance and confinement ratio are also required to be displayed. The total distance is defined by the sum of the Euclidean distances computed from the first frame when the cell was detected to the second and so on till the current frame. The net distance is defined by the Euclidean distance between the cell's coordinates in the frame and its coordinates in the first detected frame. The confinement ratio is defined by the ratio of the total distance to the net distance of the cell.

II. LITERATURE REVIEW

Automated cell tracking methods generally involve two main steps: segmenting individual cells and associating cells over time [1]. Methods for segmenting individual cells include region growing, watershed, and edge-based segmentation techniques [2]. In recent years, deep learning techniques are also applied to segment individual cells in images [3, 4, 5]. The simplest method to associate cells over time is to associate cell with the spatially nearest detected cell in the previous frame [1]. More robust methods consider a combination of cell features instead of just spatial distance [6].

Various kinds of computer vision techniques are used to perform cell segmentation. Usually, this process starts with using image pre-processing techniques to expose and contrast the cells from the background. The techniques include variations of thresholding [2], top-hat filtering, and h-maxima transformation [6]. For some cases, ridge detection filter is used to highlight the boundaries of the cells [8]. After the pre-processing step, the cells are segmented using techniques such as region growing, watershed, edge-based segmentation techniques, and template-matching [1, 2].

Different segmentation techniques might produce different results and encounter different problems. The watershed technique is prone to over-segmentation [1]. There

exist methods to avoid it, but only works for some cases [9]. Ellipse-fitting has been used as an alternative to the watershed that is able to avoid over-segmentation [6]. Template-matching techniques encounter problems when there are variations in cell morphology [1]. Techniques based on deep learning, especially convolutional neural networks such as U-net, requires an annotated training set [5].

There are various kinds of cell association method in automated cell tracking. As mentioned, the simplest approach is to associate the spatially nearest segmented cell in the previous frame [1]. This approach can be made more robust by generalizing the meaning of "near" to be "similar". Instead of just calculating spatial distance, some methods combine various similarity measures to decide association, such as motion skewness, cell area, colour, and shape deformation [6]. Probabilistic schemes are also another approach to increase the robustness of cell association [1].

Tracking contour evolution is also an alternative option for automated cell tracking [7]. This method segments the cells only in the first image of the sequence. Then, they fit a contour to the edge of each segmented cells. The contours then evolved throughout the image sequence to associate the same cells and track their movement. However, this method is only able to work under the assumption that there is an unambiguous overlap between regions of the same cell in both previous and current frames [10].

Various approaches are taken to detect cell mitosis in microscopic image sequences. One of the techniques is recovering broken trajectory of the movement of the cells [6]. For some cases, a good approach is to use a probabilistic model to detect a mitosis event [11]. Deep learning approaches using convolutional neural networks are also used [12, 13].

III. METHODS

This section explains the methods that we use to perform the tasks given in the project. It begins with the big picture as the first subsection presents the overview of the flow of the application. After that, subsequent subsections lay out the operations that we apply at a single frame of the sequence, such as pre-processing, segmentation, cell association, and mitosis detection. Lastly, the last subsection explains how we acquire and calculate the cell metrics for task 3.

A. Application Flow Overview

The beginning stage of the application starts from listing the frames in the sequence until displaying the first frame to the user interface window. First, the specified directory of the frame sequence is read in order to get a list of images in the sequence. Then, the user interface window is initialized and set up. Next, it reads the first frame in the sequence, pre-processes it, and segments the individual cells in the image. Each cell is assigned an ID number and has its original coordinates recorded. The number of identified cells and detected mitosis events are counted and recorded. Lastly, the frame is displayed to the user interface window with green coloured boxes drawn on the boundary of the segmented cells.

Each subsequent frame is applied with the same operations from it is loaded until it is displayed, as illustrated in Figure 1. First, the application loads the frame, pre-process it and segment the cells in it. After that, each segmented cell is associated with an identified cell in the previous frame and any mitosis event is detected and recorded. The number of identified cells and the number of detected mitosis events are also recorded. Then, boxes are drawn on the boundary of each identified cell and lines are drawn representing the movement of each cell. Lastly, the frame, cell counts, mitosis counts, bounding boxes, and movement trails are displayed to the user interface window. Then, the application loads the next frame in the sequence, perform the same operations, and so on until all frames in the sequence has been loaded, processed, and displayed.

The user is able to interact at any time with the application when it is running. The user can pause the application so it will not proceed with loading and processing the next frame until the application is resumed. When the user left-clicks at any segmented cell, the metrics of the clicked cell at that particular frame are shown in the user interface window.
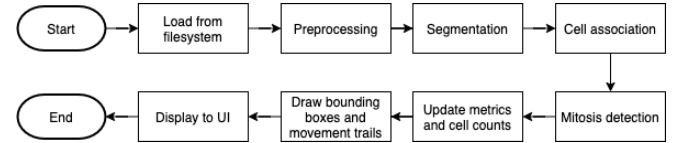

Figure 1. Operations applied to each frame following the first frame.

When all of the frames in the sequence have been processed and displayed, the user is able to reset the application and start from the beginning by clicking the rerun button.

B. Pre-processing

Pre-processing steps are applied with the aim to expose the cells and contrast them with the background so that they can be easily segmented. Most of the pre-processing steps are different for each image set because each image set has different characteristics. For Fluo-N2DL-HeLa, simple global thresholding is enough to contrast the cells with the background. On the other hand, we have to apply white top-hat transform followed by Otsu's thresholding to PhC-C2DL-PSC images to ease the segmentation of this image set. DIC-C2DH-HeLa is the most difficult to segment because the grey intensities of the body of the cells are mostly the same as the background. Hence, for this image set, we specifically apply a ridge filter to expose the boundary of the cells. All images go through the same finishing pre-processing steps, which are morphological opening and morphological closing. This is done in order to remove artefacts and noise.
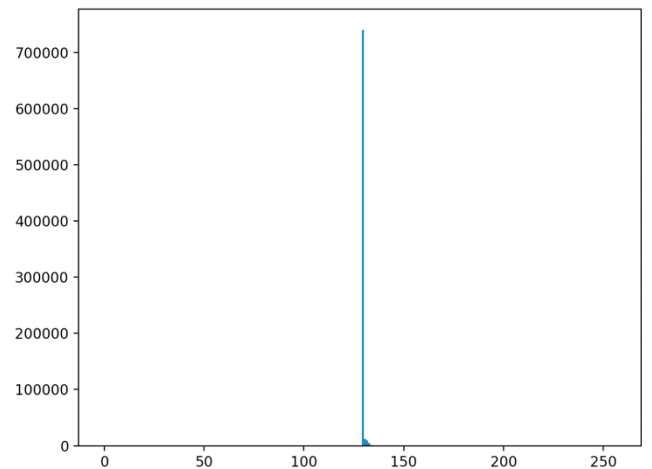

Figure 2. Typical intensity histogram of a Fluo-N2DL-HeLa image.

Pre-processing for Fluo-N2DL-HeLa images is simpler because of the characteristic of their grey intensity distribution. A typical intensity histogram of a Fluo-N2DL-HeLa image is shown in Figure 2. As we can see from the histogram, most of the pixels have the same grey intensity,
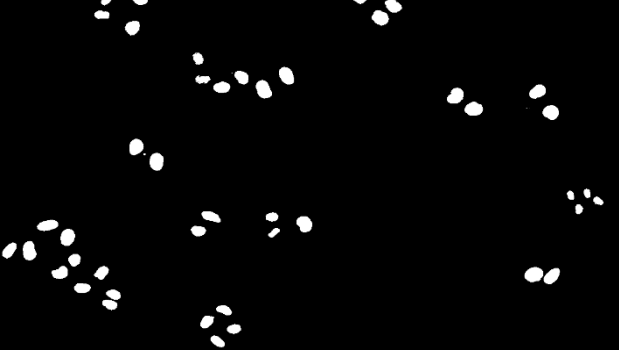

Figure 3. Result of global thresholding of a Fluo-N2DL-HeLa image with threshold 129.

which is 128, while the rest have higher intensity. Because most of the pixels in the image are background pixels, we suspect that the pixels whose grey intensity 128 are indeed the background pixels. This suspicion is vindicated because global thresholding with threshold 129 is able to differentiate the cells with the background, as illustrated in Figure 3.

PhC-C2DL-PSC images need an additional pre-processing step because illumination variation exists in them. Thresholding cannot be applied to images with nonuniform lighting because cells in darker areas have the same grey intensity as the background in lighter areas. Hence, white top-hat transform is applied to remove the effect caused by this variation in illumination, as illustrated in Figure 4a and 4(b). After that, Otsu's thresholding is applied to the image as illustrated in Figure 4(c). We use Otsu's thresholding because we cannot pinpoint a reliable threshold value for each image as in the case of Fluo-N2DL-HeLa. Figure 4(d) shows the result of Otsu's thresholding before white top-hat transform.
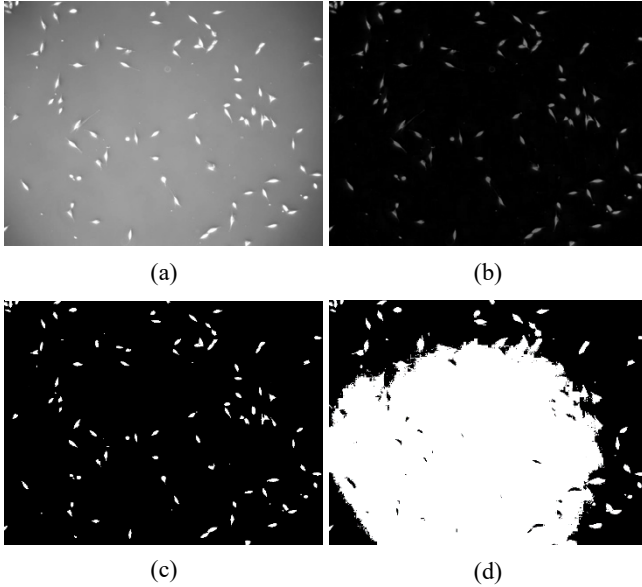

Figure 4. Illustration of pre-processing steps for PhC-C2DL-PSC images. (a) The original image before pre-processing. (b) Result of white top-hat transform to the original image. (c) Result of Otsu's thresholding after white top-hat transform. (d) Result of Otsu's thresholding before white top-hat transform.

From that image, we can see that applying white top-hat transform is indeed an important pre-processing step for this image set.

We take a different approach to pre-processing DIC-C2DH-HeLa images. We have to do that because the grey intensity of the body of the cells is more or less the same with the background, as illustrated in Figure 5(a). Inspired by [8], we decided to use a ridge filter from the scikit-image package, frangi, to extract the boundaries of the cells. The resulting image of the filter is then linearly contrast-stretched to contrast the boundaries of the cells with the background and the body of the cells, as illustrated in figure 5(b). Lastly, because we
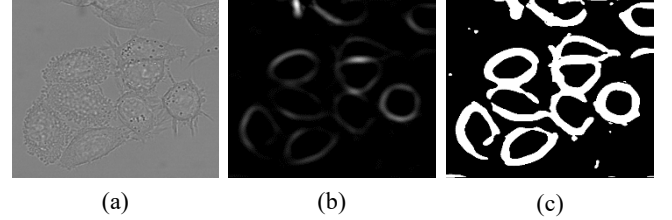

Figure 5. Illustration of pre-processing steps for DIC-C2DH-HeLa. (a) The original image. (b) Contrast-stretched result of applying a ridge filter to the image. (c) The binary image resulted from thresholding the ridge-filtered image.

need a binary image for segmentation, global thresholding with threshold 5 is applied to the image. This threshold value is decided by experimenting with different threshold values to find a reasonable value that captures most of the boundaries of the cell while not capturing many artefacts from the background. The thresholding result is shown in Figure 5(c).

Morphological opening and closing are applied at the end of pre-processing steps for images in each imageset. These operations are essential in removing artefacts captured by previous pre-processing steps. We find that these operations are effective in removing some artefacts in all three image sets. Figure 6a and 6b illustrate the effect of these morphological operations.

Figure 6. Illustration of the effect of morphological operations to a Fluo-N2DL-HeLa image after thresholding. (a) Before morphological operations, artefacts are seen in the image. (b) After morphological operations, the artefacts have been removed.

C. Segmentation

We use the ellipse-fitting method to segment individual cells in the image. First, we use the Canny edge detector to get a binary image representing the edges of the cells. Then, we find external contours corresponding to the boundaries of the cells on the binary image using OpenCV's findContour() function with RETR_EXTERNAL as the retrieval method. Lastly, we fit ellipses to the contours using OpenCV's fitEllipse() function. Each fitted ellipse is counted as a segmented individual cell.

We have experimented with watershed segmentation, but we find that ellipse-fitting method is superior to the watershed
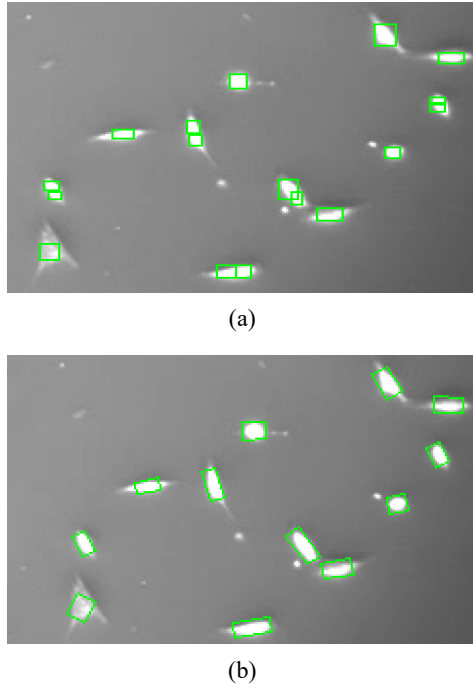
(a)

(b)

Figure 7. Comparison of segmentation using ellipse-fitting and using the watershed method on a PhC-C2DL-PSC image. (a) Watershed segmentation result, which contains some over-segmentations. (b) Result of segmentation using ellipse-fitting, which is able to avoid over-segmentations.

for the image sets given in this project. Watershed segmentation results in many over-segmentations, especially for image sets that have irregular cell shape like PhC-C2DL-PSC. In those cases, we find that ellipse-fitting is able to avoid over-segmentations, as illustrated in Figure 7. Also, the result of the pre-processing steps that we apply for DIC-C2DH-HeLa is not compatible with watershed segmentation.

Segmentation for DIC-C2DH-HeLa images requires an additional post-processing step. The pre-processing operations on these images do not satisfactorily remove notable artefacts from the image. Moreover, the ellipse-fitting operation sometimes produces a large ellipse encompassing the whole image that does not represent the actual cell. Hence, after segmentation, we explicitly reject fitted ellipses that are too small or too large compared to the estimated size of the cells. Specifically, we reject ellipses with an area less than 1/100 of the image area or greater than 1/5 of the image area.

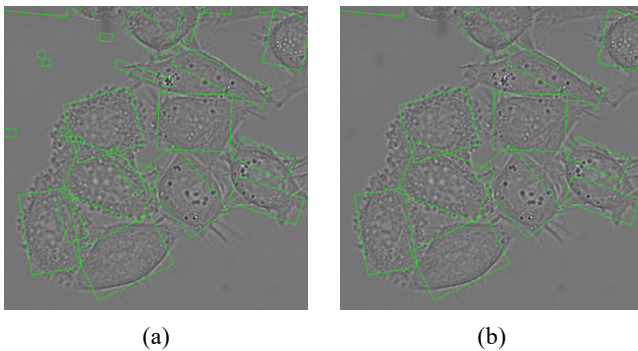(a)   (b)

Figure 8. Illustration of the effect of an additional post-processing step to the segmentation of a DIC-C2DH-HeLa image. (a) Segmentation result without additional post-processing. (b) Segmentation result with additional post-processing.
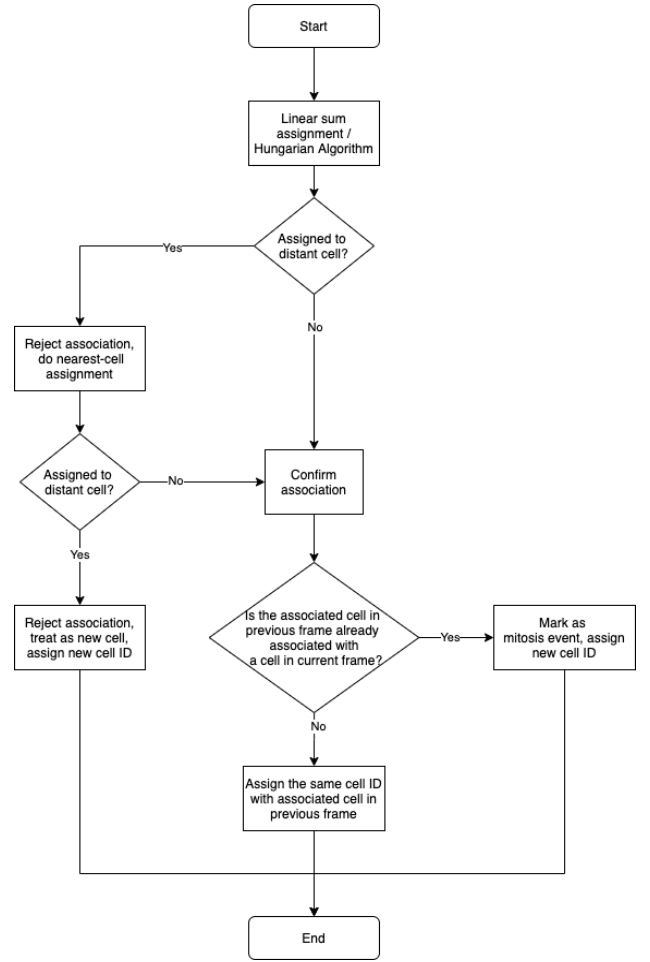

Figure 9. Flow chart describing the implemented scheme for cell association and mitosis detection.

We find that this additional step improves the segmentation result, as illustrated in Figure 8.

D. Cell Association and Mitosis Detection

We had thought of associating cells by performing SIFT keypoint matching between image frames. The intention was to let SIFT do the cell association so that we only have to handle the case when there are differing number of cells in consecutive frames. The difference being attributed to either occlusion or mitosis. However, we quickly found out that SIFT couldn't match properly because of too many moving entities. Also, sometimes it would identify multiple keypoints in a cell. This posed association challenges. We couldn't find the right parameters to limit the number of keypoints identified and realised that a distance-based method is needed instead.

We implemented a simple nearest-neighbour based scheme to associate cells and to detect mitosis events, as illustrated in Figure 9. This scheme consists of two-pass assignments of cells of the current frame with cells of the previous frame. The first pass uses a modified Hungarian algorithm that rejects assignments of cells that are considerably distant from each other. The leftover cells that do not get assigned in the first pass will go through the second pass. In the second pass, each cell is simply assigned to the nearest cell in the previous frame, though the association between distant cells is also rejected. As a consequence of this second pass, it is possible that a single cell in the previous

frame to be associated with two or more cells in the current frame. This event is considered as a mitosis event.

In the first pass of the scheme, we use a modified Hungarian algorithm to assign each cell in the current frame to a cell in the previous frame. First, the spatial distance between each cell in the current frame and each cell in the previous frame is calculated. This distance value is used as the measure of cost to decide the cheapest overall assignment by the Hungarian algorithm. We reject any assignment whose distance between assigned cells is above a threshold. The thresholds are the ratio between the distance and the diagonal of the image, which are decided by the estimating the reasonable distance of the movement of the cells in each image set. They are 0.1 for DIC-C2DH-HeLa, 0.025 for Fluo-N2DL-HeLa, and 0.01 for PhC-C2DL-PSC. Each assignment resulted from the Hungarian algorithm whose distance below the threshold is confirmed and the assigned cell in the current frame is assigned the same cell ID as the associated cell in the previous frame.

The purpose of the second pass of the scheme is to assign remaining cells that are not assigned the first pass while detecting mitosis events. In this pass, each remaining unassigned cell is assigned to its nearest cell in the previous frame, regardless of whether the nearest cell has been assigned to another cell in the first pass or not. Note that we also reject assignments with distance above a threshold, with the same threshold as in the first pass. If the nearest cell has not been assigned to another cell, then association proceeds identically to associations in the first pass. On the other hand, if the nearest cell has been assigned to another cell, then we consider this as a mitosis event. If a cell is considered to be originated from a mitosis event, we mark it as such, then the cell is assigned a new cell ID.

We also handle remaining cells that are still unassigned in the second pass. Any unassigned remaining cells after the second pass are considered new cells. These cells are given a new cell ID and their metrics calculation starts from that point. We consider these cells to be cells that just come into the view of the microscope image at that frame or are under-segmented in the previous frame. Lastly, some cells in the previous frame might not be assigned to any cells in the current frame. We ignore these cells because we consider these cells to be cells that get outside of the view of the microscope image at the current frame or a result of over-segmentation.

E. Metrics Measurement and Calculation

In this project, the application must be able to display four metrics of a selected cell at any frame. The metrics are speed, total distance, net distance, and confinement ratio. To acquire the value for speed and total distance metrics, the application records the displacement of a cell at each frame. The speed is the displacement of the cell for the current frame, while the total distance is the sum of all displacements from the first frame the cell appears to the current frame. In order to acquire the value for net distance, the application records the coordinate of a cell at the first frame the cell appears. The net distance is the distance between the recorded original coordinate of the cell to its coordinate at the current frame. Lastly, the confinement ratio is simply the ratio between the total distance and the net distance metrics of a cell.

IV. EXPERIMENTAL SETUP

Due to limited time and resources, we conducted a simple experiment to evaluate the application in three aspects: segmentation, mitosis detection, and cell association. For segmentation and mitosis detection, we manually inspect 5 frames from each image set to evaluate the accuracy of segmentation and mitosis detection performed by the application. On the other hand, we evaluate the cell association performance of the application by considering the number of cells that are failed to be associated with each frame. We acknowledge that these evaluation methods are not robust and not perfect. However, this is the best that we can come up with considering the limited time and resources that we have.

As mentioned, we conducted a simple manual experiment to evaluate cell segmentation and mitosis detection performance of the application. For each image set, we take the segmentation and mitosis detection result of 5 arbitrary frames. For each of the 5 frames, we manually count the number of observed cells and the number of observed mitosis events. Then, we calculate the difference between the manually observed count with the count produced by the application. The error is defined as the ratio between the aforementioned calculated difference to the manually observed count, both for segmented cell count and mitosis event count. We average this error over the 5 inspected frames.

In order to evaluate cell association, we consider the number of segmented cells that have failed to be associated with each frame. There are some reasons why some cells do not get associated with any cell from the previous frame or the next frame. One of the reasons is that the movement distance of a cell is above the set threshold at that frame so that the application erroneously considers it two different cells. Another reason is that the segment that we consider to be a cell is a result of over-segmentation or under-segmentation in the previous frame and that the segmentation error is fixed in the current frame. There is also a possibility that the Hungarian algorithm erroneously assigns different cells because there is no guarantee that the nearest cell in the previous frame is the actual same cell. Hence, the evaluation is based on the average ratio of the number of cells that are failed to be associated with the total number of segmented cells at each frame. We are able to conduct this cell association evaluation automatically because the application has access to these values.

V. RESULTS AND DISCUSSION

A. Cell Segmentation Evaluation Results

Table I presents the results of cell segmentation evaluation experiments. The table shows the manually observed cell count, automated cell count, the error or difference between the observed count and the automated count, and the ratio of the error to the observed cell count for each inspected frame of each image sets. The higher the ratio of the error to the observed cell count, the worse the cell segmentation performance. The average error and the average ratio of error to the observed cell count of each three given image sets are also calculated and shown on the table. The bar chart in Figure 10 compares the average error ratios of each image set.

Imageset	Seq.	Frame	Man. Count	Auto. Count	Error	Error Ratio
Fluo	1	4	39	36	3	0.0769
Fluo	1	21	51	50	1	0.0196
Fluo	2	7	145	139	6	0.0414
Fluo	3	25	83	85	2	0.0241
Fluo	3	10	55	56	1	0.0182
Fluo Avg.					**2.6**	**0.0360**
PhC	1	3	82	80	2	0.0244
PhC	1	21	84	79	5	0.0595
PhC	2	21	82	81	1	0.0122
PhC	3	7	81	79	2	0.0247
PhC	3	19	85	83	2	0.0235
PhC Avg.					**2.4**	**0.0289**
DIC	1	2	12	13	1	0.0833
DIC	1	25	12	12	0	0.0000
DIC	2	14	9	12	3	0.3333
DIC	3	2	10	1	9	0.9000
DIC	3	18	12	9	3	0.2500
DIC Avg.					**3.2**	**0.3133**

calculated. The average ratio overall for 4 sequences in each image sets are also calculated. The bar chart in Figure 11 compares the average association failure rates of each image set.

TABLE II.   Average Ratio of Cell Association Failures

Seq.	Fluo-N2DL-HeLa	PhC-C2DL-PSC	DIC-C2DH-HeLa
1	0.0177	0.0686	0.2827
2	0.0253	0.0605	0.2798
3	0.0180	0.0549	0.2437
4	0.0176	0.0630	0.1887
Overall	**0.0196**	**0.0618**	**0.2487**

Figure 11. Bar chart that compares the average association failure rate of each imageset.

As we can see from the table, the average ratio of association failure for Fluo-N2DL-HeLa images is considerably low (around 2%). We think the reason for this is that Fluo-N2DL-HeLa images are very easy to segment accurately because the cell shapes are relatively consistent and their pre-processing steps are able to accurately separate the cells from the background. Moreover, the movement of the cells in this image set is stable and not erratic. Hence, the average ratio of cell association failure of this image set is relatively low.

The average ratio of association failure for PhC-C2DL-PSC image set is higher than the average ratio of association failure for Fluo-N2DL-HeLa, though still relatively low (around 6%). We think that the reason that the value is relatively higher than the value of Fluo-N2DL-HeLa is that, there are some artefacts in this image set that move quickly across the view of the microscope. These artefacts are sometimes incorrectly segmented as cells. The distance of their movements is well above the distance threshold for cell association. Hence, this causes a relatively high number of association failure for this image set.

On the other hand, the average ratio of association failure for DIC-C2DH-HeLa images is considerably high (around 25%). We expect this high error rate because the images in DIC-C2DH-HeLa images are very tough to segment. As mentioned, the grey intensity of the body of the cells is more or less the same with the background. Hence, we have to apply additional steps for pre-processing and segmentation for this image set. However, we admit that the pre-processing and segmentation methods that we apply for this image set are far from perfect. We tried multiple algorithms like level set and watershed but they could not perform well. Hence, many
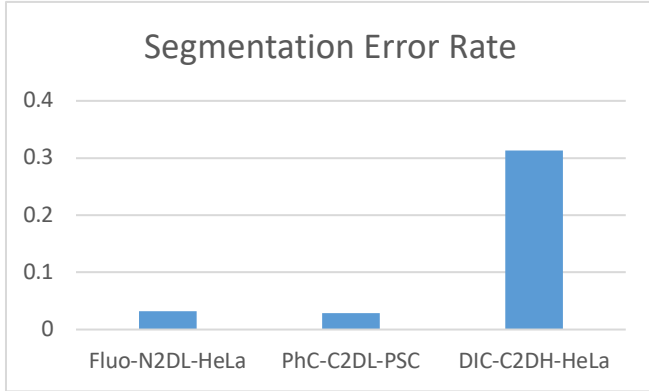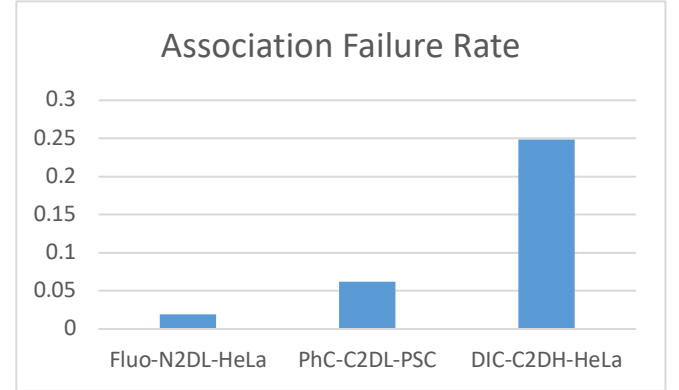

Figure 10. Bar chart that compares the average segmentation error ratios of each imageset.

The results show that cell segmentation error ratio for Fluo-N2DL-HeLa and PhC-C2DL-PSC image sets is relatively low (around 3-4%), while the error ratio for DIC-C2DH-HeLa image set is considerably high (around 31%). Segmentation error for Fluo-N2DL-HeLa and PhC-C2DL-PSC image sets is relatively low because the pre-processing steps have already produced a clear and accurate separation between the cells and the background. Hence, segmentation for these image sets is straightforward and more accurate. On the other hand, the cell segmentation error ratio for DIC-C2DH-HeLa images is very high because the pre-processing steps are unable to produce a binary image that is easy to segment accurately. Consequently, erroneous segmentation results are more common in the DIC-C2DH-HeLa images.

B. Cell Association Evaluation Results

The results of cell association evaluation experiments are presented in Table II. The values are the average ratio of the number of cells that have failed to be associated with the total number of segmented cells at each frame. The higher the value, the worse the cell association performance. The average ratio for each sequence of the three given image sets is

segmentation errors occurred that affect cell association performance.

C. Mitosis Detection Evaluation Results

Table III shows the results of mitosis detection evaluation experiments. The table shows the manually observed cell count, the number of manually observed mitosis events, the number of detected mitosis events, the error or difference between the observed mitosis count and detected mitosis count, and the ratio of the error to the number of cells in each observed frame of each image sets. The higher the ratio of the error to the number of cells, the worse the mitosis detection performance. The average error and the average ratio of error to the number of cells of each three given image sets are also calculated and shown on the table. The bar chart in Figure 12 compares the average ratio of mitosis detection error to cell count for each image set.

TABLE III.   MITOSIS DETECTION EVALUATION RESULTS

Image set	Seq.	Frame	Cell Count	Man. Count	Auto. Count	Error	Error Ratio
Fluo	1	4	39	2	2	0	0.0000
Fluo	1	21	51	4	0	4	0.0784
Fluo	2	7	145	5	3	2	0.0138
Fluo	3	25	83	2	3	1	0.0120
Fluo	3	10	55	0	1	1	0.0000
Fluo Avg.						**1.6**	**0.0209**
PhC	1	3	82	3	0	3	0.0366
PhC	1	21	84	5	0	5	0.0595
PhC	2	21	82	0	1	1	0.0123
PhC	3	7	81	0	0	0	0.0000
PhC	3	19	85	1	0	1	0.0118
PhC Avg.						**2.0**	**0.0240**
DIC	1	2	12	2	2	0	0.0000
DIC	1	25	12	2	2	0	0.0000
DIC	2	14	9	0	1	1	0.1111
DIC	3	2	10	1	0	1	0.1000
DIC	3	18	12	0	3	3	0.2500
DIC Avg.						**1.0**	**0.0922**

The results show that the ratio of mitosis detection errors to the number of cells is relatively lower in Fluo-N2DL-HeLa and PhC-C2DL-PSC image sets (around 0.02), while the average ratio of mitosis detection errors to the number of cells
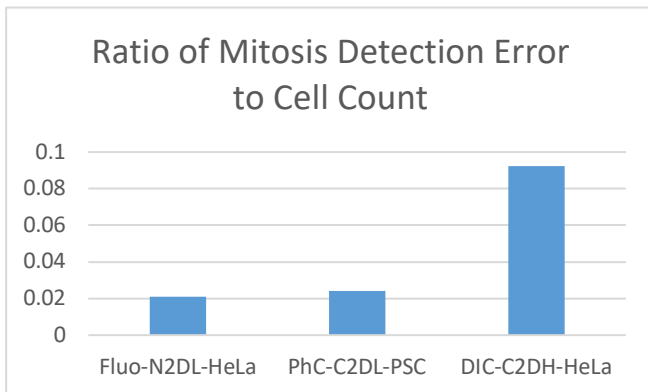
Figure 12. Bar chart that compares the average ratio of mitosis detection error to cell count for each imageset.

of the DIC-C2DH-HeLa images is relatively higher (around 0.09). Consistent with the evaluation results of cell segmentation and cell association, the average error ratio is relatively higher in DIC-C2DH-HeLa images than the average error ratios of the other two image sets. As previously mentioned, DIC-C2DH-HeLa images are tough to segment accurately because of the characteristics of its images in addition to pre-processing steps that are unable to produce a binary image that is easy to segment. Hence, segmentation errors are more common in this image set, which causes higher mitosis detection error rate.

VI. CONCLUSION

The results of the experiments for all three aspects that are evaluated show that the error rates in Fluo-N2DL-HeLa and PhC-C2DL-PSC image sets are low. However, the error rate in DIC-C2DH-HeLa images is considerably higher than the other two image sets. From these results, we can conclude that our pre-processing, cell segmentation and cell association methods work well for Fluo-N2DL-HeLa and PhC-C2DL-PSC images. However, we can also conclude that our methods do not work well for the DIC-C2DH-HeLa images.

We recommend further research on how to track cells in the DIC-C2DH-HeLa images accurately. We support approaches that are radically different than our approach for this image set because the result of our approach is not satisfactory and suffers from a high error rate. Hence, small modifications to our approach might not considerably improve the results. We think that approaches based on supervised learning might be a good solution to track cells in DIC-C2DH-HeLa images and worth further study.

In addition, we also recommend further work to improve our cell association and mitosis detection scheme. Our cell association scheme is able to be made more robust by considering similarity measures other than just spatial distance of the segmented cells. Lastly, our mitosis detection scheme could be improved by considering the change in the shape or size of the cell during mitosis.

VII. CONTRIBUTION OF GROUP MEMBERS

Jatin Gupta worked on preprocessing, watershed segmentation, evaluation of the algorithms, report, slides, and communication channel between students and tutor.

Karan Inder Singh worked on preprocessing, level set segmentation using Geodesic Active Contour (GAC) of level set method, presentation slides, and the report.

Marhadiasha Kusumawardhana worked on preprocessing, ellipse-fitting segmentation, mitosis detection, metrics measurement, user interface of the application, and the report.

Shubhankar Mathur worked on morphological operations for preprocessing, cell association using Hungarian algorithm, experimented SIFT keypoints matching for cell association.

Yash Tamakuwala worked on preprocessing, cell association scheme (experimented with SIFT keypoints matching and Hungarian algorithm), and the report.

VIII. REFERENCES

[1]   E. Meijering, O. Dzyubachyk, I. Smal, W. A. van Cappellen. "Tracking in cell and developmental biology". *Seminars in Cell and Developmental Biology*, vol. 20, no. 8, pp. 894-902, October 2009, 10.1016/j.semcdb.2009.07.004.

[2] J. Rogowska. "Overview and Fundamentals of Medical Image Segmentation," in *Handbook of Medical Imaging*. I. Bankman, Ed., Cambridge, MI, USA: Academic Press, 2000.

[3] Y. Al-Kofahi, A. Zaltsman, R. Graves, *et al*. "A deep learning-based algorithm for 2-D cell segmentation in microscopy images," *BMC Bioinformatics*, vol. 19, October 2018, Art. no. 365, doi: 10.1186/s12859-018-2375-z.

[4] J. B. Lugagne, H. Lin, M. J. Dunlop. "DeLTA: Automated cell segmentation, tracking, and lineage reconstruction using deep learning," *PLoS Computational Biology*, vol. 16, no. 4, April 2020, doi: 10.1101/720615.

[5] O. Ronneberger, P. Fischer., T. Brox. "U–Net: Convolutional Networks for Biomedical Image Segmentation," in *Lectures Notes in Computer Science*, vol. 9351, Cham, Switzerland: Springer, 2015, doi: 10.1007/978-3-319-24574-4_28.

[6] M. A. A. Dewan, M. O. Ahmad and M. N. S. Swamy, "Tracking Biological Cells in Time-Lapse Microscopy: An Adaptive Technique Combining Motion and Topological Features," in *IEEE Transactions on Biomedical Engineering*, vol. 58, no. 6, pp. 1637-1647, June 2011, doi: 10.1109/TBME.2011.2109001.

[7] N. Ray and S. T. Acton, "Active contours for cell tracking," in *Proceedings Fifth IEEE Southwest Symposium on Image Analysis and Interpretation*, Sante Fe, NM, USA, 2002, pp. 274-278, doi: 10.1109/IAI.2002.999932.

[8] K. E. G. Magnusson, J. Jaldén, H. M. Blau, "KTH-SE", March 2020. Acessed: July 31, 2020. [Online]. Available: https://public.celltrackingchallenge.net/participants/KTH-SE.pdf

[9] W. Bieniecki, "Oversegmentation avoidance in watershed-based algorithms for color images," in *Proceedings of the International Conference Modern Problems of Radio Engineering, Telecommunications and Computer Science, 2004.*, Lviv-Slavsko, Ukraine, 2004, pp. 169-172, doi: 10.1109/TCSET.2004.1365910

[10] V. Ulman, M. Maška, K. Magnusson, *et al*. "An objective comparison of cell-tracking algorithms, " *Nature Methods*, vol. 14, no. 1141-1152, 2017, doi: 10.1038/nmeth.4473.

[11] S. Huh, D. F. E. Ker, R. Bise, M. Chen and T. Kanade, "Automated Mitosis Detection of Stem Cell Populations in Phase-Contrast Microscopy Images," in *IEEE Transactions on Medical Imaging*, vol. 30, no. 3, pp. 586-596, March 2011, doi: 10.1109/TMI.2010.2089384.

[12] Y. Zhou, H. Mao, Z. Yi, "Cell mitosis detection using deep neural networks, " *Knowledge-Based Systems*, vol. 137, pp. 19-28, December 2017, doi: 10.1016/j.knosys.2017.08.016.

[13] Y. Li, E. Mercan, J. G. Elmore, L.G. Saphiro "Efficient and Accurate Mitosis Detection - A Lightweight RCNN Approach" in *Proceedings of the 7th International Conference on Pattern Recognition Applications and Methods – Volume 1: ICPRAM*, pp. 69-77, 2018, doi: 10.5220/0006550700690077.